

## Enhanced Characterisation Studies and Synthesis of Undoped and Copper Doped-Organic Nonlinear Optical Single Crystal: L-Alanine Aluminium Nitrate

Anand Kumar Pandey,<sup>1</sup> Raghvendra Pratap Singh,<sup>1\*</sup>  
Ahmed Hussain Jawhari<sup>2</sup> and Ritu Singh<sup>3</sup>

<sup>1</sup>Department of Chemistry, Kamla Nehru Institute of Physical and Social Sciences, Sultanpur-228118, India

<sup>2</sup>Department of Chemistry, Faculty of Science, Jazan University, P.O. Box 2097, Jazan, Saudi Arabia

<sup>3</sup>Department of Chemistry, S.S.V. P.G. College, Hapur-245101, India

\*Corresponding author: [drpsinghdrpsingh@gmail.com](mailto:drpsinghdrpsingh@gmail.com)

Published online: 6 December 2023

To cite this article: Pandey, A. K., et al. (2023). Enhanced characterisation studies and synthesis of undoped and copper doped-organic nonlinear optical single crystal: L-alanine aluminium nitrate. *J. Phys. Sci.*, 34(3), 117–134. <https://doi.org/10.21315/jps2023.34.3.8>

To link to this article: <https://doi.org/10.21315/jps2023.34.3.8>

**ABSTRACT:** *Single crystals of untreated and copper (Cu<sup>2+</sup>) metal ion-doped L-alanine aluminium nitrate (LAAN), a room-temperature slow evaporation organic nonlinear optical material. Single crystals were studied for structural, spectral, optical, hardness, second-order non-linear optical, electrical [(alternating current (AC) and direct current (DC)], and photoconductivity properties as they grew. Crystallinity, monoclinic structure with space collection P<sub>21</sub>, and lattice specifications were deliberate using single crystal X-ray diffraction investigation. The existence of functional clusters is revealed by the spectral properties, and the means of vibration of various molecular clusters existing in LAAN were evaluated using Fourier transform infrared (FTIR). The low cut-off wavelength and transmittance properties were determined using optical analysis. The band gap energy of LAAN and Cu-doped LAAN crystals was estimated to be 3.40 eV and 2.70 eV, respectively, using the Tauc plot. It was revealed that pure crystals had a lower dielectric constant than crystals that had been doped with copper. After doping with rising temperatures, AC conductivity started to rise. With the use of the Kurtz and Perry approach, the effectiveness of the grown crystal's second harmonic generation was computed, Cu-doped LAAN was discovered to be 3.3 times more prominent than potassium dihydrogen phosphate (KDP) and 2.2 times more prominent than pure LAAN crystals. The nonlinear optical characteristics of LAAN crystals have therefore been improved by copper doping. It is*

*most suited for use in electro-optic applications like laser technology, telecommunications and optical signal processing because of its negative photoconductivity.*

**Keywords:** LAAN single crystals, copper, non-linear optical material, second harmonic generation (SHG)

## 1. INTRODUCTION

The most significant field of science and technology is crystal growth. A significant field of research in crystal engineering and materials is the creation of compounds based on metal-organic frameworks.<sup>1</sup> Among them, nonlinear optical (NLO) materials are crucial for the development of cutting-edge modern technologies, including telecommunication, signal processing, data storage, super-resolution lithography, and microscopy as well as higher harmonic and terahertz (THz) generation.<sup>2-4</sup> The next generation of integrated photonic circuits is expected to use NLO materials, specifically those with well-defined designs on the (sub)wavelength length scales.<sup>5,6</sup> NLO materials have attracted a lot of attention lately due to their applications in lasers, optical transfers, mixing and rearranging, data repositories, and electro-optic programming.<sup>7</sup> Due to their greater nonlinearity than traditional inorganic materials, organic constituents that can be used in NLO tools are in high demand. Complexes of amino acids have recently been explored.<sup>8,9</sup> Amino acids have the potential to be useful materials in NLO applications. Since all amino acids have chiral uniformity and crystallise in non-centrosymmetric space clusters, they are crucial in NLO applications.<sup>10</sup> Numerous natural amino acids have NLO properties due to their chiral carbons, a proton-donating carboxyl (-COOH) group, and a proton-accepting amino (-NH<sub>2</sub>) group.<sup>11</sup> The neutral alanine molecule is composed of zwitterions, which means that the carboxyl group has been dissociated and the amino group has been protonated. Hence, salts of L-arginine, L-histidine and L-alanine were formed with various organic/inorganic acids.<sup>12</sup> L-alanine compounds have received far less attention and are likely to form a more stimulating material. Recently, several novel complexes containing the amino acid L-alanine have been crystallised, and their structural, optical and thermal properties have all been studied.<sup>13</sup> As a result, enhanced research is needed to understand the consequence of various types of adulteration on the physical specifications of this material. The crystal structure of L-alanine in 1:1 and 2:1 nitric acid ratio has already been reported.<sup>14</sup> At room temperature, we employed a gradual evaporation strategy in this study to grow divalent metal particles Cu<sup>2+</sup> doped and pure LAAN single crystals from an aqueous solution. The properties of obtained or grown single crystals were examined. The results of the characterisation show that Cu-doped LAAN single crystal has superior dielectric, electrical and NLO assets to another dopant.

## 2. EXPERIMENTAL

### 2.1 Crystal Analysis

LAAN was created by combining L-alanine and nitric acid in a 2:1 stoichiometric ratio and adding double-distilled water to it. A considered quantity of copper (II) chloride ( $\text{CuCl}_2$ ) additives were mixed into the LAAN solution to make doped LAAN. Separate preparations were made for the pure and doped LAAN solutions and thoroughly dissolved in double distilled water before being thoroughly stirred in ambient conditions for about 4 h with a magnetic stirrer to ensure homogeneous temperature and concentration over the entire volume of the solution with pH set to 2.5. Both solutions were heated to  $50^\circ\text{C}$  to obtain pure and doped LAAN salts (in separate beakers). The filtered solution was then transferred to crystal growth containers, where it crystallised via steady evaporation at room temperature. The salt was then repeatedly crystallised to remove impurities.<sup>15</sup> Transparent, colourless solo crystals of LAAN were obtained over the course of 10 days. Figure 1 displays images of LAAN single crystals that are both pure and doped.

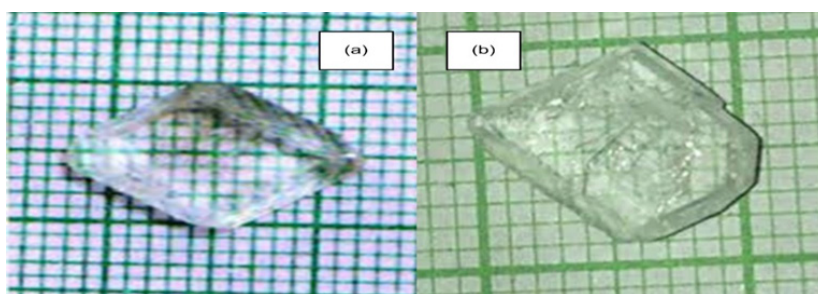


Figure 1: Picture of grown crystals (a) Pure LAAN and (b) Cu-doped LAAN.

L-alanine ( $\text{CH}_3\text{CHNH}_2\text{COOH}$ ) and nitric acid ( $\text{HNO}_3$ ) were combined in a 2:1 stoichiometric ratio to produce LAAN.<sup>16</sup> The following process was used to determine the appropriate amounts of L-alanine and nitric acid:



The crystal's chemical structure (Figure 2) is shown below:

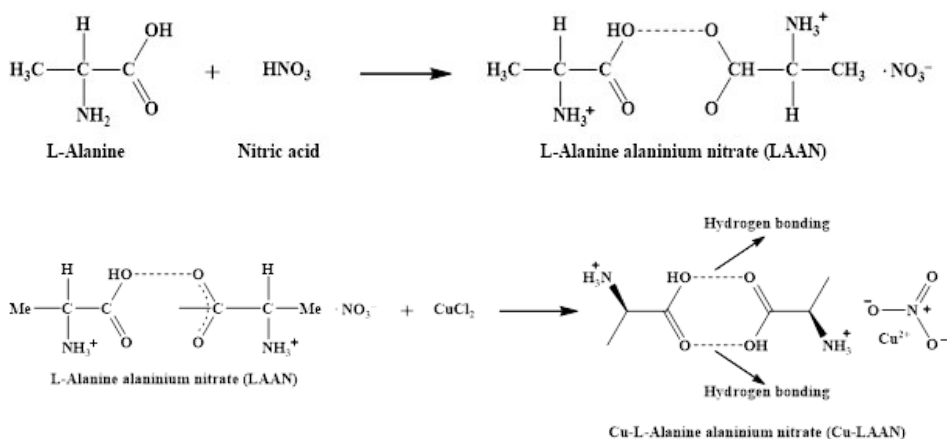


Figure 2: Crystal's chemical structure.

## 2.2 Characterisations

Utilising industry-standard software, the powder X-ray diffraction pattern was used to determine the cell characteristics of the formed crystal. Both pure and doped single crystals were crushed and filtered through a sieve with a micron aperture to create powders with uniform particle sizes. They were then examined using a Panalytical Powder X-ray diffractometer (Germany) with nickel-filtered  $\text{CuK}$  radiation (35 kV, 30 mA) to perceive how  $\text{Cu}^{2+}$  doping affected the LAAN crystal system and lattice specifications. Under the same experimental conditions, entire samples were scanned at room temperature for an angle range of  $10^\circ$  to  $60^\circ$  of  $2\theta$  at a scan rate of 0.001/s. Following the KBr pellet technique, Fourier transform infrared (FTIR) examination applying a BRUKER 66V FT-IT spectrometer (USA) in the range  $4,000\text{ cm}^{-1}$  to  $400\text{ cm}^{-1}$  confirmed the association of L-alanine with nitric acid. To study the optical transparency of the grown crystals, UV-vis spectra in the wavelength range of 200 nm to 1100 nm were noted employing a Lambda 35 UV-Vis-NIR spectrometer (Canada). For the current investigations, single crystals of pure and doped LAAN (thickness 2 mm) were cut and polished. One of a crystal's most vital strength specifications is hardness, and this trial is non-destructive. A  $5\text{mW}$   $\text{Ar}^+$  ion laser operating in the 490 nm area with a power density of  $0.125\text{ Wcm}^{-2}$  was used to handle the photoluminescence spectrometer. The Perkin Elmer LS 55 luminescence spectrometer (Waltham, USA) was used to record the photoluminescence spectrum for the LAAN single crystal. The current study's excitation wavelength is 390 nm. The hardness of a substance is a range of its resistance to permanent deformation of the lattice.

Utilising an optical microscope and a Vickers diamond pyramidal indenter-equipped microhardness tester (HMV-2) (Maharsahtra, India), the microhardness of the crystal was assessed. The microhardness value was calculated using loads ranging from 10 g to 100 g. Radical cracks develop as a result of mechanical contact between the impression and the crystal facet. With a HIOKI 3532-50 LCR meter (Japan), dielectric dimensions were made between 100 kHz and 2 MHz. Without light, a Keithley 485 pico ammeter (Japan) was utilised to analyse the photoconductivity calculations. The Kurtz powder method was applied [second harmonic generation (SHG)] to ascertain the sample's second harmonic generation.

### 3. RESULTS AND DISCUSSION

#### 3.1 Powder X-ray Diffraction Analysis

Figure 3 displays the powder X-ray diffraction gratings of  $\text{Cu}^{2+}$  doped and undoped LAAN crystals. It was discovered that the intensity of a few reflections, such as (2 0 0), (1 0–4) and (3 0 0), increased. This shows that the  $\text{Cu}^{2+}$ -doped KDP's overall crystallinity has increased. The characteristic peaks of the pattern do not vary as  $\text{Cu}^{2+}$  concentration rises, but the intensity of the peaks related to (2 0 0) constantly rises and achieves peak value. This peak's elevated potency could be attributed to plane surface enlargement caused by the rapid production of planes normal to it in the existence of dopant molecules.<sup>17,18</sup> Engrossed dopant molecules on the facet also make impurity molecules entering the crystalline matrix more difficult, resulting in higher ideal crystalline. Pure and  $\text{Cu}^{2+}$  doped KDP crystals have remarkably similar crystallographic parameters, validating that the single crystal included the monoclinic structure with the space group of  $\text{P}_{21}$  as shown in Table 1. This clearly shows that  $\text{Cu}^{2+}$  doping affects crystal morphology but not crystal structure. LAAN's crystal structure is unaffected by the dopant material. Lattice strain caused by dopants in LAAN crystals changes the unit cell parameters of the doped samples.<sup>19</sup> The substitution or arrangement of the smaller lattice  $\text{Cu}^{2+}$  molecule by the larger LAAN molecule caused a slight rise in the lattice specifications and unit cell volume of LAAN crystals, allowing the lattice to be strained.<sup>20</sup>

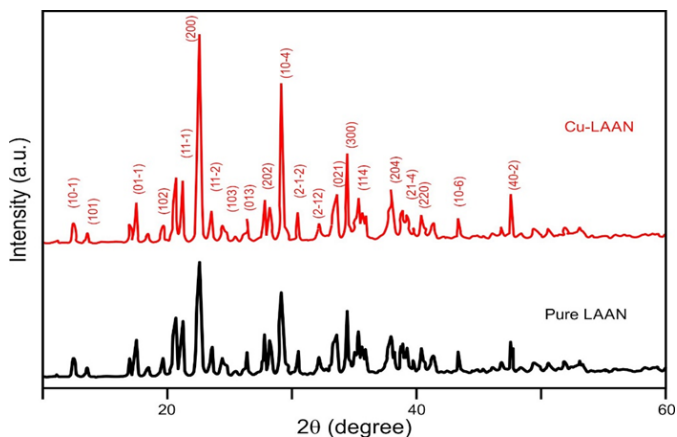


Figure 3: Powder XRD pattern of pure LAAN and Cu-doped LAAN.

Table 1: Lattice (a,b,c) specifications of untreated and Cu<sup>2+</sup> doped LAAN crystals.

LAAN crystals	Lattice parameters				Volume (Å <sup>3</sup> )
	a (Å)	b (Å)	c (Å)	β (°)	
Reported	7.851	5.441	12.806	94.05	544.81
Pure LAAN	7.835	5.344	12.890	94.15	545.43
Cu <sup>2+</sup> -doped LAAN	7.876	5.545	12.989	94.38	559.21

### 3.2 Vibrational Spectral Analysis

To determine whether the crystals have functional groups, FTIR spectrum synthesis of both untreated and doped LAAN crystals was performed between 400 cm<sup>-1</sup> and 4000 cm<sup>-1</sup> in the middle infrared (IR) regions. The FTIR frequencies of clear LAAN crystal are shown in Figure 4. The N-H stretch of NH<sup>3+</sup> creates a broad, strong band in the higher energy area. Because of the hydrogen bonding between NH<sup>3+</sup> and COO<sup>-</sup> into the crystal lattice of pure LAAN, the band's lower energy region has a delicate structure. The detected bands resulting from fundamental vibration are compatible with the evidence that has been published.<sup>21-23</sup> The hydrogen bonding of the NH<sup>3+</sup> and COOH groups was responsible for the ascent, a great spike was experienced in the range 2110.19 cm<sup>-1</sup> to 2112.12 cm<sup>-1</sup>. CH<sub>3</sub> has bending modes at 1359.86 cm<sup>-1</sup> to 1361.79 cm<sup>-1</sup> and 1503.38 cm<sup>-1</sup> to 1510.31 cm<sup>-1</sup>. C-O stretch causes the 1411.94 cm<sup>-1</sup> peak, as does the COOH group's O-H bend at 1232.55 cm<sup>-1</sup> to 1234.48 cm<sup>-1</sup>. The IR spectra shows that nitric acid protonates the COO<sup>-</sup> of both untreated and doped LAAN. There exists

a minor movement in the absorption bands when the IR spectra of both untreated and doped LAAN are evaluated, which may be the result of mixing.<sup>24</sup> Table 2 shows the vibration values of both untreated and Cu-doped LAAN single crystals.

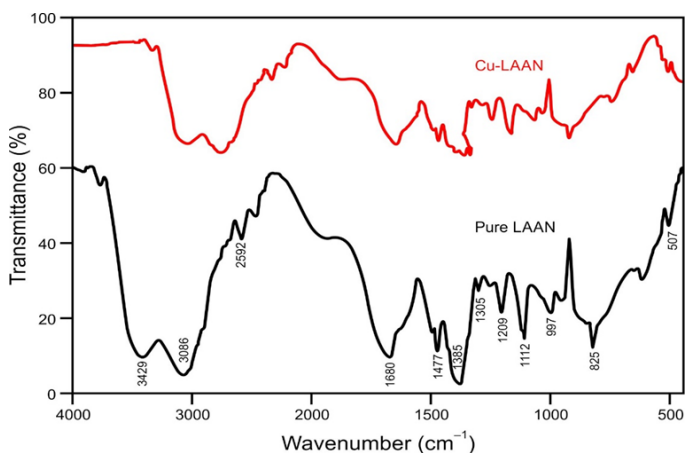


Figure 4: FTIR spectroscopy analysis of pure and Cu-doped LAAN single crystals.

Table 2: Vibration values of both pure and Cu-doped LAAN single crystals.

Peak range		Intensity	Vibrations
Untreated/ pure LAAN	Cu-doped LAAN		
3429	3440	Broadband	OH elongating vibration of COOH group
3086	3109	Sharp and intense	NH elongating vibration of NH <sub>3</sub> group
2592	2602	Weak	Methyl and methane group C-H vibrations
1680	1685	Broadband	C-O elongating of COOH group
1477	1477	Sharp	CH <sub>3</sub> flexing modes and NH <sub>3</sub> expanding modes
1385	1390	Sharp and broadband	CH <sub>3</sub> flexing modes and COO <sup>-</sup> symmetric vibrations
1305	1305	Small and weak	NO <sub>3</sub> <sup>-</sup>
1209	1209	Sharp	COO <sup>-</sup> vibrations
997	999	Sharp and small	NO <sub>3</sub> <sup>-</sup> group
825	820	Small and weak	NO <sub>3</sub> <sup>-</sup> group

### 3.3 UV-Vis Spectral Investigation

The optical relaying range and visibility cut-off are extremely significant optical specifications for laser frequency conversion devices, any NLO material must have a wide transparency window to remain efficient, hence the transmission spectra are crucial.<sup>25</sup> The UV-Vis broadcasting of both untreated and doped LAAN crystals was measured, in addition, the design that resulted is revealed in Figure 5(a). When differentiated from pure LAAN, the transmission ratios of doped samples were discovered to be significantly higher.

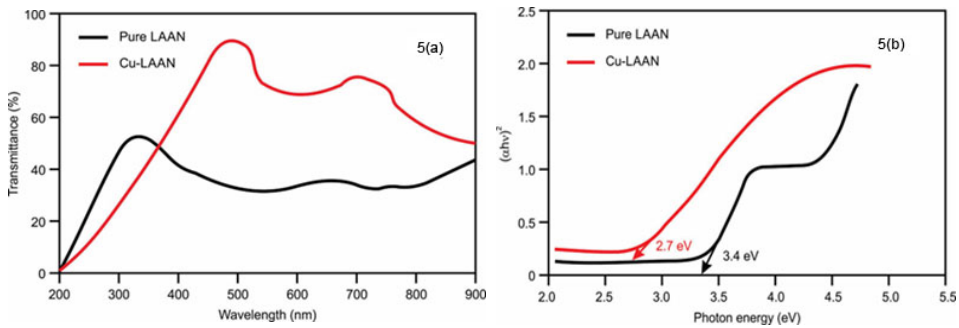


Figure 5: Pure and Cu-doped LAAN crystals (a) Transmittance spectrum; and (b) Band gap energy graph.

According to a spectral examination of UV, both pure and doped LAAN crystals exhibit effective relaying in the UV and visible regions, which is advantageous for optoelectronic applications.<sup>26</sup> According to the transmittance spectrum, the crystal seems to have a narrow UV cut-off of 320 nm for untreated or pure LAAN, however, the band moves to the higher wavelength side of 480 nm to 490 nm following the integration of the  $\text{Cu}^{2+}$  metal ions.<sup>27</sup>

The dependence of the optical absorption coefficient with the photon energy helps to study the band structure and the type of transition of electrons. The optical absorption coefficient was calculated from the transmittance using the following relation.

$$\alpha = \log(1/T)/t \quad (2)$$

where T is the transmittance and  $t \sim 1.0$  mm is the thickness of the crystal. Owing to the direct band gap, the crystal under study has an absorption coefficient ( $\alpha$ ) obeying the following relation for high photon energies (hv):

$$\alpha = A (hv - E_g)^{1/2} / hv \quad (3)$$

where  $E_g$  stands for the optical band gap of the crystal and  $A$  is a constant. Figure 5(b) depicts the  $(h\nu)^2$  vs  $h\nu$  variation.<sup>28</sup> The linear part is extrapolated to calculate  $E_g$ . A significant redshift is caused by a decline in the crystals' optical band gap energy. Using the Tauc plot (Figure 5b), both LAAN and doped Cu LAAN crystals were projected to have band gaps of 3.4 eV and 2.7 eV, respectively.<sup>29</sup> As a result, the UV results indicate that Cu-doped LAAN might efficiently expand absorption and reduce electron-hole pair recombination, both of which considerably increase SHG effectiveness.<sup>30</sup>

### 3.4 Photoluminescence Spectral Analysis

For the pure and Cu-doped LAAN single crystals illustrated in Figure 6, the photoluminescence spectra were conducted in the 300 nm to 650 nm area. A significant concentration of protonation of amino groups to carboxyl groups occurs in the 425 nm area. It was abundantly clear that pure LAAN crystals had a higher photoluminescence (PL) emission intensity than doped LAAN crystals. The presence of dopants steadily decreased the intensity of the PL emission.<sup>31</sup> Particularly, a notable decrease in PL intensity was seen in Cu-doped LAAN single crystals. This can be the result of stopping the process of electron-hole pair recombination.<sup>32</sup> As a result, the UV and PL results reveal that Cu-doped LAAN might greatly increase SHG efficiency by successfully improving the absorption property and suppressing the electron-hole pair's recombination process.<sup>33</sup>

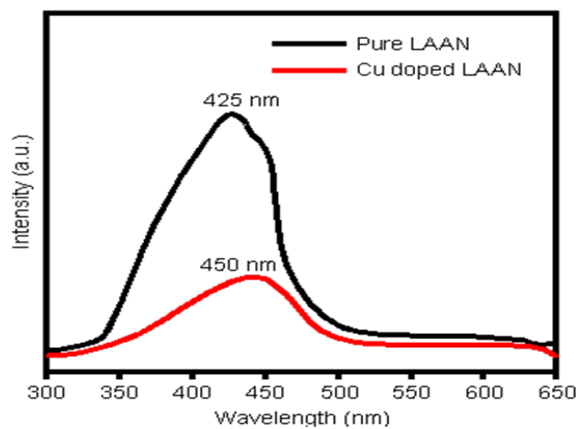


Figure 6: Photoluminescence spectra of pure and Cu-doped LAAN crystals.

### 3.5 Microhardness Studies

In relation to the aforementioned NLO applications, crystals must also have good mechanical toughness (or mechanical characteristics), which is important in device manufacture. It is an ability of a material's resistance to scratch-induced localised plastic deformation.<sup>34</sup> A smooth and flat facet of both untreated and Cu-doped LAAN crystals of identical dimension was chosen for room temperature hardness testing through a Leitz-Wetzlar hardness tester furnished with a diamond square indenter. The following relationship remained used to calculate hardness (HV) values:  $HV = 14.8544P = d^2$ , where P is the load in kilograms and d is the mean diagonal length in mm.<sup>35</sup> The micro-hardness of the grown crystals was determined by dividing the applied load by the indentation surface area. This was done for each load with a different indentation surface area. The average of these surface areas was used to calculate the crystal's micro-hardness.<sup>36,37</sup> Figure 7 depicts the variations in hardness HV for pure and doped crystals with load P ranging from 10 g to 100 g. The graph shows that the hardness of all crystals increases linearly as the load increases up to 100 g without cracking. When compared to pure material, doping increases the strength of the material by exhibiting high resistance to dislocation motion. The higher micro-hardness values of the Cu-doped crystals indicate that the dopant enters the LAAP crystal lattice and possibly forms additional bonds with their neighbouring LAAP atoms, necessitating more stress to form dislocations and a greater push to form parting, confirming additional significant crystalline flawlessness. As a result, Cu-doped LAAP crystals are more mechanically suitable for device fabrication.<sup>38</sup>

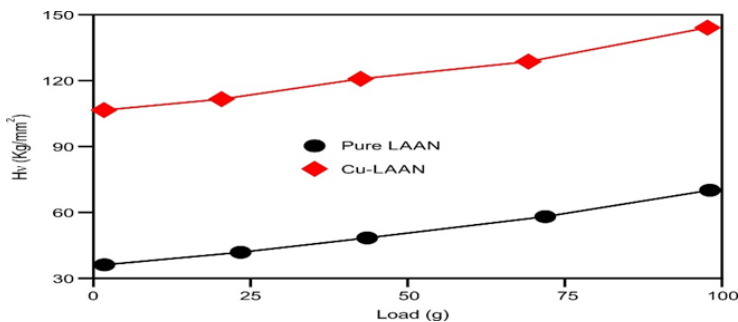


Figure 7: Microhardness study of both Untreated and Cu-doped LAAN crystals.

### 3.6 Dielectric Analysis of Untreated and Doped LAAN Crystals

The above-mentioned facets of the specimens were coated with a silver paste to generate communication between the crystal and the copper electrodes. A rectangular sample of both untreated and doped LAAN crystals is used for

dielectric experiments. Plots of the dielectric constant vs frequency for LAAN crystals that are both pure and doped are shown in Figure 8. For both untreated and doped LAAN crystals, the dielectric constant falls with increasing frequency and stays virtually constant in the high-frequency zone. The idea of polarisation can be used to describe this. It is anticipated that polarisation will occur as a result of the local electron displacement caused by the electronic exchange of ions in crystals in the direction of the applied field. As the frequency of the applied field rises, the space charge polarisation is unable to maintain itself and adapts to the variation of the external field, resulting in a decrease in polarisation. Prior studies established the values of the dielectric constant and dielectric loss.<sup>39</sup> Figure 8(a), (b) and (c) depicts the frequency response of the dielectric loss in both pure and doped crystals. This graph demonstrates that as frequency rises, the dielectric loss falls for all samples. It is also evident that doped crystals experience larger dielectric loss at lower frequency regions than pure crystals.<sup>40</sup> A sample with low dielectric loss at high frequency indicates that it has good optical value with fewer flaws, and this specification is critical for NLO materials in their application.<sup>41</sup>

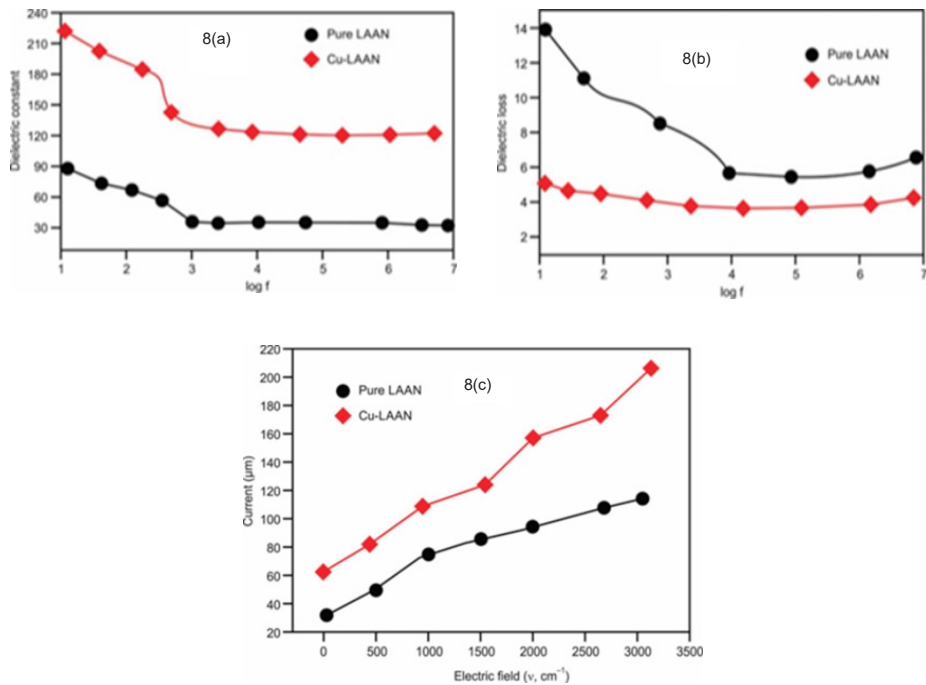


Figure 8: Represents the dielectric study of pure LAAN and Cu-doped LAAN single crystals (a) Dielectric constant; (b) Dielectric loss; and (c) Dielectric current.

### 3.7 AC Conductivity

The image depicts how metal-doped and pure LAAN single crystals behave in terms of conductivity, and this electrical conductivity experiment was conducted between 30°C and 90°C. Figure 9 demonstrates how the AC conductivity of all specimens rises with temperature and rises at all temperatures following doping. At room temperature, a constant frequency of 1 kHz was used to test the AC transfer competence of both untreated and doped crystals. The defect concentration rises exponentially with temperature, increasing electrical conductivity.<sup>42</sup> According to the data, Cu-doped LAAN crystals are more conductive than untreated LAAN crystals. As shown in Figure 9(a), the electric conductivity at room temperature of untreated LAAN and Cu-doped LAAN single crystals is 1.40 and 5.21  $\text{Xm}^{-1}$ , respectively. The initiation energy was considered by using the Arrhenius relation by plotting  $1000/T$  versus  $\log$  conductivity.<sup>43</sup> Figure 9(b) depicts the activation energies considered by the slope of the  $1000/T$  versus  $\ln r$  plot.<sup>44</sup> We conclude here that after doping, the activation energy decreases. When Cu impurities were added to LAAN crystals, the lattice defects increased, increasing conductivity and thus decreasing activation energy which is found to be 0.45 (pure LAAN) and 0.22 (Cu-doped LAAN).<sup>45,46</sup>

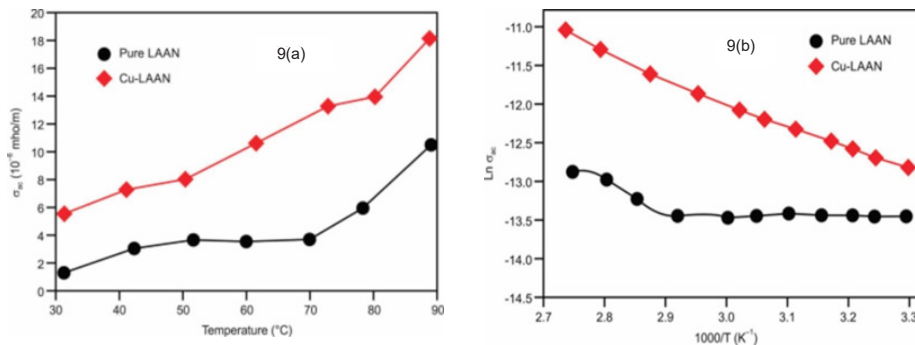


Figure 9 (a) AC electrical conductivity versus temperature for pure and Cu-doped LAAN crystals; and (b) variation of  $\ln(r)$  with  $1000/T$  of pure and Cu-doped LAAN crystals.

### 3.8 Photoconductivity

A photoconductivity study was conducted for Cu-doped LAAN single crystals and the dim current was measured for all the growth crystals. Figure 10 shows the variety of both dull current ( $I_d$ ) and photocurrent ( $I_p$ ) with the connected electrical field. The plot clearly shows a connection to the electric field and the  $I_d$  and  $I_p$  current test straightly increased. The plot above plot denotes dim current is continuously

more important than the photocurrent, and it confirms the presence of negative photoconductivity. The negative photoconductance (NPC) effect, defined as an increase in resistance upon exposure to illumination, holds great potential for application in photoelectric devices.<sup>47</sup> In contrast to positive photoconductivity, NPC refers to a phenomenon in which conductivity decreases under illumination. It has novel application prospects in the field of optoelectronics, memory, gas detection, etc.<sup>48</sup>

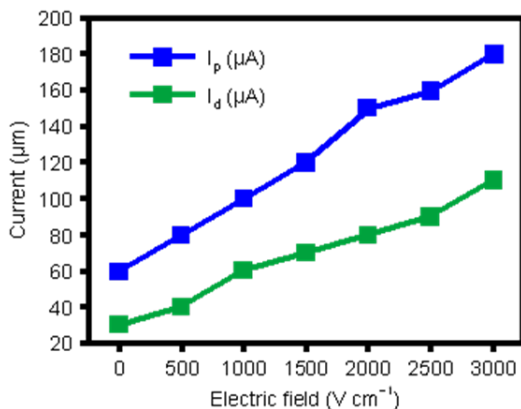


Figure 10: Field-dependent photoconductivity of Cu-doped LAAN single crystals.

### 3.9 SHG Competence Test

Using a modified Kurtz and Perry setup, calculations were made to determine the SHG high yield of both pure and doped LAAN crystals. With a recurrence rate of 10 Hz, a 1064 nm -switched Nd: YAG laser beam with an input power of 2.15 mJ and pulse width of 10 ns was used. Powdered crystals were packed into a micro-capillary with a uniform bore and subjected to laser radiation. The intensity of the 532 nm component was collected by monochromatic the output of each sample (monochromator, model Triax, 550). Randomly oriented microcrystals produced second harmonic radiation, which was focused by a lens and noticed by a photomultiplier tube (PMT, Philips Photonics, model 8563), and demonstrated on a cathode ray oscilloscope. The second harmonic generation was confirmed by the green radiation that the pure and doped LAAN crystals emitted at 532 nm (SHG). The efficacy of ordinary KDP is lower compared to that of untreated and doped LAAN crystals.<sup>49</sup> In raw and Cu-doped LAAN crystals, SHG efficacy is 2.1 substantially greater. The effectiveness of the Cu-doped LAAN single crystal is consequently 3.2 times that of other growing crystals. The enhanced SHG shows that the main element in raising the relative SHG effectiveness of LAAN is the protonation of the amino group in the L-alanine molecule.<sup>50</sup> One of the most

significant sightings of the current study is that Cu doping increases SHG output significantly. Furthermore, because Cu is metallic, it may have a higher electrical nature than pure LAAN.<sup>51</sup>

#### 4. CONCLUSIONS AND FUTURE RECOMMENDATIONS

At standard temperature, single crystals of both untreated LAAN and doped with Cu were developed slowly through the evaporation process. The lattice constants of the produced crystals were determined using X-ray diffraction analysis on a single crystal. The structural parameters of the two crystals,  $a = 7.851 \text{ \AA}$ ,  $b = 5.441 \text{ \AA}$ ,  $c = 12.806 \text{ \AA}$ ,  $\beta = 94.75^\circ$  and volume  $V = 547 \text{ \AA}^3$ , are associated with space group  $P_{21}$ . The creation of one LAAN crystal is verified using FTIR measurements. Particularly at  $\lambda = 480 \text{ nm}$ , the Cu-doped LAAN crystal UV-VIS spectrum of redshift was captivated. Single crystals created of raw LAAN had an 85% transparency, while those made of doped LAAN had a 60% transparency. The pure and doped LAAN crystal's excellent transmission properties over the visible area assure its appropriateness for SHG activities. Low dielectric constant and greater frequency dielectric loss point to increased optical characteristics in the crystals, which is crucial for NLO applications. The electric conductivity of both untreated and Cu-doped LAAN single crystals is 1.4, 5.2, 2.3 and  $3.2 \text{ X m}^{-1}$ , sequentially, according to the AC conductivity measurements. The Cu-doped LAAN crystal created through synthesis has strong fabrication potential for NLO devices and can be integrated into photonic devices (to assess applications like frequency conversion and optical modulation). Since the research is iterative, each step may generate fresh issues and lines of inquiry. It's critical to maintain a dialogue with the scientific community to acquire diverse viewpoints on the material's characteristics and future applications, which will help you develop and broaden your research in this fascinating field of nonlinear optics.

#### 5. ACKNOWLEDGEMENTS

Anand Kumar Pandey is thankful to Kamla Nehru Institute of Physical and Social Sciences for providing support for the preparation of this manuscript.

#### 6. REFERENCES

1. Christy, D. S. et al. (2022). Study of physico-chemical properties and growth dimension augmentation of barium succinate single crystals grown by slow evaporation technique. *J. Phys. Sci.*, 33(1), 29–49. <https://doi.org/10.21315/jps2022.33.1.3>

2. Vermeulen, N. et al. (2023). Post-2000 nonlinear optical materials and measurements: Data tables and best practices. *J. Phys. Photonics*, 5(3), 035001. <https://doi.org/10.1088/2515-7647/ac9e2f>
3. Zhou, L. et al. (2020). Nonlinear optical characterization of 2D materials. *Nanomaterials*, 10(11), 2263. <https://doi.org/10.3390/nano10112263>
4. Yao, C. et al. (2022). Advanced nonlinear optical materials and devices. *Front. Phys.*, 10, 1025019. <https://doi.org/10.3389/fphy.2022.1025019>
5. Semin, S. et al. (2021). Nonlinear optical properties and applications of fluorenone molecular materials. *Adv. Opt. Mater.*, 9(23), 2100327. <https://doi.org/10.1002/adom.202100327>
6. Chen, C.-T. & Liu, G.-Z. (1986). Recent advances in nonlinear optical and electro-optical materials. *Ann. Rev. Mater. Sci.*, 16, 203–243. <https://doi.org/10.1146/annurev.ms.16.080186.001223>
7. Blanc, W. et al. (2023). The past, present and future of photonic glasses: A review in homage to the United Nations International Year of glass 2022. *Progr. Mater. Sci.*, 134, 101084. <https://doi.org/10.1016/j.pmatsci.2023.101084>
8. Marder, S. R. (2006). Organic nonlinear optical materials: Where we have been and where we are going. *Chem. Commun.*, 131–134. <https://doi.org/10.1039/B512646K>
9. Liang, H. et al. (2023). Nanoencapsulation-induced second harmonic generation in pillararene-based host–guest complex cocrystals. *J. Am. Chem. Soc.*, 145(5), 2870–2876. <https://doi.org/10.1021/jacs.2c10674>
10. Mendiratta, S. et al. (2015). Metal-organic frameworks for electronics: Emerging second-order nonlinear optical and dielectric materials. *Sci. Technol. Adv. Mater.*, 16(5), 054204. <https://doi.org/10.1088/1468-6996/16/5/054204>
11. Radhika, S. et al. (2012). Thermal, optical, mechanical, and electrical properties of a novel NLO active glycine potassium sulphate single crystals. *Der Pharma Chemica*, 4(5), 2014–2023. DPC-2012-4-5-2014-2023-libre.pdf
12. Nugrahani, I. & Jessica, M. A. (2021). Amino acids as the potential co-former for co-crystal development: A review. *Molecules*, 26(11), 3279. <https://doi.org/10.3390/molecules26113279>
13. Kotelnikova, E. et al. (2020). Limits of solid solutions and thermal deformations in the L-alanine–L-serine amino acid system. *Crystals*, 10(7), 618. <https://doi.org/10.3390/cryst10070618>
14. Hudson, M. R. et al. (2009). Inelastic neutron scattering and Raman spectroscopic investigation of L-alanine alaninium nitrate, a homologue of a ferroelectric material. *Phys. Chem. Chem. Phys.*, 11, 9474–9483. <https://doi.org/10.1039/B905070A>
15. Aravindan, A. et al. (2007). Investigations on the growth, optical behaviour and factor group of an NLO crystal: L-alanine alaninium nitrate. *Cryst. Res. Technol.*, 42, 1097–1103. <https://doi.org/10.1002/crat.200710954>
16. Gopalakrishnan, R. & Ramasamy, P. (2009). Reply to “Comments on papers reporting IR-spectra and other data of L-alanine alaninium nitrate and L-alanine sodium nitrate crystals” by M. Fleck and A. M. Petrosyan. *Cryst. Res. Technol.*, 44(7), 773–775. <https://doi.org/10.1002/crat.200900206>

17. Ghazaryan, V. V. et al. (2012). Structure and vibrational spectra of L-alanine L-alaninium picrate monohydrate. *J. Mol. Struct.*, 1015, 51–55. <https://doi.org/10.1016/j.molstruc.2012.02.007>
18. Krishna, D. N. G. & Philip, J. (2022). Review on surface-characterization applications of X-ray photoelectron spectroscopy (XPS): Recent developments and challenges. *Appl. Surf. Sci. Adv.*, 12, 100332. <https://doi.org/10.1016/j.apsadv.2022.100332>
19. Singh, P. et al. (2013). Investigation on growth features and crystal structures of pure and metal ion ( $Mn^{2+}$ ) doped KDP single crystals. *Optik*, 124, 1609–1613. <https://doi.org/10.1016/j.ijleo.2012.04.015>
20. Hasmuddi, M. et al. (2014). Structural, spectroscopic, optical, dielectric and mechanical study of pure and L-proline doped ammonium dihydrogen phosphate single crystals. *Spectrochim. Acta A: Mol. Biomol. Spectrosc.*, 123, 376–384. <https://doi.org/10.1016/j.saa.2013.12.038>
21. Periathai, R. S. & Rajagopal, K. (2014). FTIR and Raman vibrational investigations on the complex of pyridine with tartaric acid. *IOSR J. Appl. Phys.*, 6, 9–12. <https://doi.org/10.9790/4861-06430912>
22. Tauc, J. (1974). Amorphous and liquid semiconductors. New York: Springer. <https://doi.org/10.1007/978-1-4615-8705-7>
23. Uthrakumar, R. et al. (2010). Bulk crystal growth and characterization of nonlinear optical bithiourea zinc chloride single crystal by unidirectional growth method. *Curr. Appl. Phys.*, 10(2), 548–552. <https://doi.org/10.1016/j.cap.2009.07.018>
24. Krishnamoorthi G. & Uvaran, R. (2021). Growth and characterization of pure and metals-doped organic nonlinear optical single crystal: L-alanine alaninium nitrate (LAAN). *J. Mater. Sci.: Mater. Electron.*, 32, 3979–3988. <https://doi.org/10.1007/s10854-020-05140-6>
25. Singh, P. et al. (2013). Investigation on structural, optical, thermal, mechanical and dielectric properties of L-proline cadmium chloride monohydrate single crystals: An efficient NLO material. *Mater. Chem. Phys.*, 142, 154–164. <https://doi.org/10.1016/j.matchemphys.2013.06.051>
26. Kanagasabapathy, K. & Rajasekaran, R. (2012). Growth, structural, optical and thermal studies of L-Threonine added Zinc(Tris) Thiourea Sulphate single crystals. *J. Optoelect. Adv. Mat.*, 6, 218–224.
27. Singh, P. et al. (2018). Enhancement of electro-optic and structural properties of TGS single crystals on doping with L-glutamic acid. *J. Mater. Sci.: Mater. Electron.*, 29: 7904–7916. <https://doi.org/10.1007/s10854-018-8790-0>
28. Avit, D. A. et al. (2019). Effects of biopolymer surfactants on the morphology and optical properties of zinc sulphide (ZnS) nanocrystalline thin film. *J. Phys. Sci.*, 30(3), 191–206. <https://doi.org/10.21315/jps2019.30.3.12>
29. Parimaladevi, R. et al. (2010). The effect of nitric acid ( $HNO_3$ ) on growth, spectral, thermal and dielectric properties of triglycine sulphate (TGS) crystal. *Spectrochim. Acta A: Mol. Biomol. Spectrosc.*, 75, 617–623. <https://doi.org/10.1016/j.saa.2009.11.027>

30. Moitra, S. & Kar, T. (2007). Growth and characterization of nonlinear optical crystal zinc tris(thiourea) sulphate in presence of L-arginine. *Opt. Mater.*, 30(3), 508–512. <https://doi.org/10.1016/j.optmat.2006.12.009>
31. Dwivedi, A. et al. (2022). Tunable photoluminescence and energy transfer of  $\text{Eu}^{3+}, \text{Ho}^{3+}$ -doped  $\text{Ca}_{0.05}\text{Y}_{1.93-x}\text{O}_2$  nanophosphors for warm white LEDs applications. *Sci. Rep.*, 12(1), 5824. <https://doi.org/10.1038/s41598-022-09630-x>
32. Shraavan, S. et al. (2017). Unusual photoluminescence of Cu–ZnO and its correlation with photocatalytic reduction of Cr(VI). *Bull. Mater. Sci.*, 40(7), 1415–1420. <https://doi.org/10.1007/s12034-017-1496-8>
33. Morales–Saavedra, O.G. & Chavira, E. (2023). Synthesis–dependent structural and optoelectronic properties of semicrystalline  $\text{LiNbO}_3:\text{SiO}_2$  hybrid silicates. *Opt. Mater.*, 142, 113930. <https://doi.org/10.1016/j.optmat.2023.113930>
34. Mao, W. G. et al. (2011). Deformation behavior and mechanical properties of polycrystalline and single crystal alumina during nanoindentation. *Scripta Mater.*, 65(2), 127–130. <https://doi.org/10.1016/j.scriptamat.2011.03.022>
35. Hasmuddi, M. et al. (2015). *Ab-initio* study of L-tartaric acid (LTA) single crystal for NLO application. *Opt. Laser Technol.*, 74, 53–59. <https://doi.org/10.1016/j.optlastec.2015.05.013>
36. Peter, M. E. & Ramasamy, P. (2016). Structural, growth and characterizations of NLO crystal: Triglycinium calcium nitrate. *Adv. Mater. Lett.*, 7(1), 83–88. <https://doi.org/10.5185/amlett.2016.5944>
37. Peter, M. E. et al. (2020). Studies of cerium doped L-alanine alaninium nitrate NLO crystal. *Int. J. Sci. Res.*, 9(3), 829–832. <https://doi.org/10.21275/SR20313222827>
38. Sirdeshmukh, D. B. et al. (2003). Systematic hardness measurements on mixed and doped crystals of rubidium halides. *Bull. Mater. Sci.*, 26(2), 261–265. <https://doi.org/10.1007/BF02707801>
39. Pandurangan, K. & Suresh, S. (2014). Synthesis, growth, and characterization of bisglycin hydrobromide single crystal. *J. Mater.*, 2014, 362678. <https://doi.org/10.1155/2014/362678>
40. Divya, N. K. et al. (2015). Dielectric properties of  $\text{Er}^{3+}$  doped ZnO nanocrystals. *Adv. Mater. Phys. Chem.*, 5(8), 287–294. <https://doi.org/10.4236/ampc.2015.58028>
41. Mechrgui, I. et al. (2022). Mixed ionic and electronic conduction in  $\text{TeO}_2\text{-ZnO-V}_2\text{O}_5$  glasses towards good dielectric features. *Materials*, 15(21), 7659. <https://doi.org/10.3390/ma15217659>
42. Jiang, J. et al. (2022). Effects of Sb doping on electrical conductivity properties in fine-grain KNN-based ferroelectric ceramics. *Crystals*, 12, 1311. <https://doi.org/10.3390/cryst12091311>
43. Joshi, C. B. & Chaudhri A. K. (2022). Sol-gel-derived Cu-Doped ZnO thin films for optoelectronic applications. *ACS Omega*, 7(25), 21877–21881. <https://doi.org/10.1021/acsomega.2c02040>
44. Vyazovkin, S. (2020). Activation energies and temperature dependencies of the rates of crystallization and melting of polymers. *Polymers*, 12(5), 1070; <https://doi.org/10.3390/polym12051070>

45. Wang, Y. et al. (2022). Recent progress on the effects of impurities and defects on the properties of Ga<sub>2</sub>O<sub>3</sub>. *J. Mater. Chem. C*, 10, 13395–13436. <https://doi.org/10.1039/D2TC01128J>
46. Faella, E. et al. (2022). Electric transport in few-layer ReSe<sub>2</sub> transistors modulated by air pressure and light. *Nanomaterials*, 12(11), 1886. <https://doi.org/10.3390/nano12111886>
47. Zhou, G. et al. (2021). Negative photoconductance effect: An extension function of the TiOx-based memristor. *Adv. Sci.*, 8(13), 2003765. <https://doi.org/10.1002/adv.202003765>
48. Cui, B. et al. (2021). Negative photoconductivity in low-dimensional materials. *Chinese Phys. B*, 30(2), 028507. <https://doi.org/10.1088/1674-1056/abcf41>
49. Ambhore, P. S. et al. (2014). NaCl, KCl and SrCl<sub>2</sub> doping effect on linear and nonlinear optical properties of KDP crystal. *Phys. Sci. Int. J.*, 4(10), 1340–1350. <https://doi.org/10.9734/PSIJ/2014/5778>
50. Aravindan, A. et al. (2008). A comparative study on the growth and characterization of nonlinear optical amino acid crystals: L-alanine (LA) and L-alanine alaninium nitrate (LAAN). *Spectrochim. Acta A: Mol. Biomol. Spectrosc.*, 71(2), 297–304. <https://doi.org/10.1016/j.saa.2007.12.023>
51. Kumar, S. et al. (2022). Structural, morphological, optical and magnetic studies of Cu-Doped ZnO nanostructures. *Materials*, 15(22), 8184. <https://doi.org/10.3390/ma15228184>